

1
2
3
4 **Comparative analysis of coronavirus genomic RNA structure reveals conservation in**
5 **SARS-like coronaviruses**
6
7

8 Wes Sanders^{1,2}, Ethan J. Fritch¹, Emily A. Madden¹, Rachel L. Graham⁴, Heather A. Vincent^{1,2#},
9 Mark T. Heise^{1,4}, Ralph S. Baric^{1,3}, Nathaniel J. Moorman^{1,2*}

10
11 ¹University of North Carolina at Chapel Hill, Department of Microbiology and Immunology, NC,
12 USA, ²University of North Carolina at Chapel Hill, Lineberger Comprehensive Cancer Center,
13 NC, USA, ³University of North Carolina at Chapel Hill, School of Public Health, NC, ⁴University
14 of North Carolina at Chapel Hill, Department of Genetics, NC, USA, [#]Present address:
15 Duke University, Department of Surgery, NC, USA, ^{*}Corresponding author

16
17
18
19
20
21
22
23
24
25
26

27 **Abstract**

28 Coronaviruses, including SARS-CoV-2 the etiological agent of COVID-19 disease, have
29 caused multiple epidemic and pandemic outbreaks in the past 20 years¹⁻³. With no vaccines,
30 and only recently developed antiviral therapeutics, we are ill equipped to handle coronavirus
31 outbreaks⁴. A better understanding of the molecular mechanisms that regulate coronavirus
32 replication and pathogenesis is needed to guide the development of new antiviral therapeutics
33 and vaccines. RNA secondary structures play critical roles in multiple aspects of coronavirus
34 replication, but the extent and conservation of RNA secondary structure across coronavirus
35 genomes is unknown⁵. Here, we define highly structured RNA regions throughout the MERS-
36 CoV, SARS-CoV, and SARS-CoV-2 genomes. We find that highly stable RNA structures are
37 pervasive throughout coronavirus genomes, and are conserved between the SARS-like CoV.
38 Our data suggests that selective pressure helps preserve RNA secondary structure in
39 coronavirus genomes, suggesting that these structures may play important roles in virus
40 replication and pathogenesis. Thus, disruption of conserved RNA secondary structures could be
41 a novel strategy for the generation of attenuated SARS-CoV-2 vaccines for use against the
42 current COVID-19 pandemic.

43

44 **Main**

45 Severe acute respiratory syndrome coronavirus (SARS-CoV), Middle Eastern respiratory
46 syndrome coronavirus (MERS-CoV), and SARS-CoV-2, the etiological agent of the current
47 COVID-19 pandemic, have caused widespread disease, death, and economic hardship in the
48 past 20 years¹, highlighting the pandemic potential of the CoV genus. While recently developed
49 antivirals show promise against MERS and SARS-CoV-2, further understanding of coronavirus
50 molecular virology is necessary to inform the design of more effective antiviral therapeutics and
51 vaccines^{6, 7}.

52 RNA structures in the ~30kb of single-stranded RNA⁸ genomes of Coronavirus play
53 important roles in coronavirus replication^{9, 5, 10, 11, 12, 13}. Given the length of coronavirus RNA
54 genomes, additional RNA structures likely exist that regulate CoV replication and disease¹⁴. In
55 this study, we used selective 2'-hydroxyl acylation by primer extension and mutational profiling
56 (SHAPE-MaP)¹⁵ to identify highly stable, structured regions of the SARS-CoV, MERS-CoV, and
57 SARS-CoV-2 genomes. Our results revealed novel areas of RNA structure across the genomes
58 of all three viruses. SHAPE-MaP analysis confirmed previously described structures, and also
59 revealed that SARS-like coronaviruses contain a greater number of highly structured RNA
60 regions than MERS-CoV. Comparing nucleotide variation across multiple strains of each virus,
61 we find that highly variable nucleotides rarely impact RNA secondary structure, suggesting the
62 existence of selective pressure against RNA secondary structure disruption. We also identified
63 dozens of conserved highly stable structured regions in SARS-CoV and SARS-CoV-2 that share
64 similar structures, highlighting the possible importance of these stable RNA structures in virus
65 replication.

66

67 **Stable RNA secondary structure is pervasive throughout coronavirus genomes**

68 To identify regions of significant RNA secondary structure in the genomes of MERS-
69 CoV, SARS-CoV, and SARS-CoV-2 we performed selective 2'-hydroxyl acylation analyzed by
70 primer extension and mutational profiling (SHAPE-MaP) analysis of virion-associated RNA^{15, 16}
71 (**Fig 1A-C; Supplemental Table 1**). Highly stable structured regions likely to maintain a single
72 confirmation were identified using high confidence cutoffs for SHAPE reactivity (<0.3, blue bars)
73 and of Shannon entropy (<0.04, black bars). We identified 85 highly stable regions in the
74 MERS-CoV genome (**Fig 1A**), 123 stable regions in the SARS-CoV genome (**Fig 1B**), and 139
75 stable regions within the SARS-CoV-2 genome (**Fig 1C**). Stable structured regions were present
76 throughout the coding and non-coding regions of each genome. SARS-CoV and SARS-CoV-2
77 exhibited greater RNA structuredness across their genomes compared to MERS-CoV. This was

78 not due to differences in overall GC content or bias in average SHAPE reactivity (**Supplemental**
79 **Fig 1A**). Thus, SARS-like coronavirus genomes contain greater overall stable RNA
80 structuredness than the MERS-CoV genome.

81 We used the SHAPE reactivity to create a structural model for stable RNA elements in
82 each genome (**Fig 1A-C; Supplemental Figure 5, Supplemental Table 2**). The top twenty
83 most stable structures for each virus were present in the coding region, and largely consisted of
84 hairpin and bulged stem loop structures. The most highly stable RNA structures were present in
85 the regions encoding open reading frame (ORF) ORF1a, ORF1b and Spike. The majority of the
86 most highly stable structures for all coronaviruses were present within ORF1a, while the number
87 of highly stable structures in ORF1b ranged from three in SARS-CoV to eight in MERS-CoV
88 (**Supplemental Fig 1B**). All coronaviruses had multiple highly stable structures in the Spike
89 ORF. These data highlight the pervasive presence of highly stable RNA structure throughout
90 coronavirus genomes.

91

92 **SHAPE-Map RNA structure prediction recapitulates known coronavirus structural 93 elements**

94 The RNA structural elements within the 5' and 3' UTRs of the related murine hepatitis
95 coronavirus (MHV) genome have been extensively characterized^{5, 17, 18}. Our SHAPE-MaP
96 analysis recapitulated previously described 5' and 3' UTR RNA secondary structures. Within the
97 5' UTR of MERS-CoV, SARS-CoV and SARS-CoV-2, we identified the conserved stem loop
98 (SL) SL1, SL2, SL4 and SL5ABC RNA elements (**Fig 2A**). Consistent with previous modeling⁵,
99 both SARS-like coronaviruses contained SL3 upstream of SL4, while this hairpin was absent
100 from MERS-CoV. A similar pattern was observed for structures within the 3'UTR (**Fig 2B**). Each
101 virus exhibited a bulged stem loop (BSL) structure, followed by a pseudoknot (PK) and each
102 genome ends in a long hypervariable (HVR) bulged stem loop structure, confirming the
103 conservation of these RNA secondary structures across coronaviruses.

104 Coronaviruses utilize a programmed -1 ribosomal frameshift to produce the ORF1a/1b
105 fusion protein. A stable RNA pseudoknot upstream of the frameshift position is necessary for
106 the frameshift to occur^{12, 13}, and our data supports the presence this pseudoknot in the same
107 position in all three coronaviruses (**Fig 2C**). Interestingly, the MERS-CoV two-stemmed
108 pseudoknot is distinct from the single-stemmed pseudoknot present in both SARS-like
109 coronaviruses. Together, these results demonstrate the capability of SHAPE-MaP analysis to
110 accurately identify RNA structures in coronavirus genomic RNA.

111 Transcriptional regulatory sequences (TRSs) are conserved, short sequences (6-8
112 nucleotides) within coronavirus genomes that act as cis-regulatory elements of transcription^{18, 19,}
113 ²⁰. While RNA secondary structure has been suggested plays a role in TRS regulation of
114 transcription, most TRS elements were not associated with areas of high RNA structuredness
115 (**Supplemental Fig 2A-D**). In fact, only a single TRS from MERS-CoV and SARS-CoV were
116 associated with highly structured RNA regions, while four TRSs from SARS-CoV-2 were
117 associated. Thus, TRS elements are not consistently associated with highly stable RNA
118 structures, suggesting that RNA secondary structure may not play a role in TRS recognition.

119
120 **Covariance and MUSCLE alignment analysis reveal selective pressure for coronavirus**
121 **RNA secondary structure**

122 To determine if RNA structuredness is a driver of mutational variance across virus
123 strains, we performed multiple sequence comparison by log-expectation (MUSCLE) alignment
124 analysis of 350 MERS-CoV, 141 SARS-CoV, and 1,542 SARS-CoV-2 genomes (**Supplemental**
125 **Table 3**). As a whole, highly structured regions within SARS-CoV exhibited significantly less
126 nucleotide variance than areas of lower structuredness, suggesting these regions may be under
127 higher selective pressure. There was no significant difference in nucleotide variance within
128 MERS-CoV or SARS-CoV-2 genomes, however 72.9% of highly structured regions in MERS-
129 CoV and 87.8% of highly structured regions in SARS-CoV-2 had lower variance than regions of

130 lower structuredness. Eighteen nucleotides in MERS-CoV, 3 nucleotides in SARS-CoV, and 8
131 nucleotides in SARS-CoV-2 showed significant variance across all strains and were located in
132 structured regions (**Supplemental Table 4**). Of these variants, 72% in MERS-CoV, 100% in
133 SARS-CoV, and 75% in SARS-CoV-2 occur in unpaired nucleotides in the stable RNA
134 secondary structure, suggesting that the majority of polymorphisms in highly structured regions
135 across coronavirus strains maintain RNA secondary structures.

136 We performed covariation analysis to further assess conservation of structuredness.
137 This analysis determines if two nucleotide changes occurred in tandem to conserve RNA
138 secondary structure. 21 structured regions in MERS-CoV strains, 1 structured region in SARS-
139 CoV strains, and 4 structured regions in SARS-CoV-2 strains contained significant covarying
140 nucleotide changes that conserved RNA secondary structure (**Supplemental Table 5**).
141 Together, these results suggest that regions of RNA structuredness and specific RNA
142 secondary structures are conserved within each virus family, and these structured regions may
143 be under selective pressure

144

145 **SARS-CoV-2 and SARS-CoV structured regions are highly conserved**

146 We next sought to identify conserved, highly stable RNA structures across all three
147 viruses. Surprisingly, outside of the previously described conserved 5' and 3' UTRs, we
148 identified only a single conserved structure across all three genomes, present within the RNA
149 region encoding nsp16 (**Supplemental Fig 3**). However, we found 98 areas of overlapping
150 highly structured regions when comparing only the SARS-CoV and SARS-CoV-2 genomes (**Fig**
151 **3A & Table 7**). Within conserved regions of structuredness in the coding region of the SARS-
152 CoV-2 genome we identified 65 regions that contained similar RNA secondary structures (**Fig**
153 **3B**). The majority of these structures (26 total) were within ORF1b, in contrast to the distribution
154 of the most stable structures within a respective genome (**Supplemental Fig 4**).

155 SARS-CoV and SARS-CoV-2 share a 79% sequence homology, thus, conserved RNA
156 structures may be driven by sequence homology rather than conservation of RNA secondary
157 structure (**Supplemental Table 6**). To determine which RNA structures were likely conserved
158 based on RNA secondary structure rather than sequence homology we calculated the average
159 percent nucleotide conservation between SARS-CoV and SARS-CoV-2 for each conserved
160 structure and compared this to the average nucleotide conservation of the two genomes (**Fig**
161 **3C**). Similar secondary structures that exhibit greater than average nucleotide homology are
162 likely driven by sequence homology, while similar structures that show lower than average
163 nucleotide homology are likely conserved based on preservation of RNA secondary structure.
164 We found 18 total structures (27.7%) with lower than average nucleotide homology, with
165 structure 6 showing the lowest sequence homology (59.4%). These data suggest that nearly
166 one third of conserved similar RNA secondary structures between SARS-CoV and SARS-CoV-2
167 are conserved based on RNA secondary structure.

168 Lastly, we assessed nucleotide covariation within conserved SARS-like CoV RNA
169 secondary structures. SARS-CoV-2 genomes were compared to MERS-CoV and SARS-CoV
170 strains and covarying nucleotides that support SARS-CoV-2 structures were identified
171 (**Supplemental Table 5**). In line with a lack of structure conservation, no MERS-CoV strains
172 showed covarying nucleotides that supported SARS-CoV-2 structures. In contrast, we identified
173 10 significant covariation events within SARS-CoV genomes that supported SARS-CoV-2
174 structures, two of which occurred within the viral UTRs. Five covariation events were observed
175 in non-conserved regions of structuredness, while three covariation events occurred within
176 conserved regions of structuredness. These results show that conservation of specific RNA
177 structures may extend outside of conserved regions of structuredness, and overall highlight the
178 high degree of structural conservation between SARS-CoV and SARS-CoV-2.

179

180 **Discussion**

181 Using SHAPE-MaP analysis we found that members of the *Coronaviradae*, MERS-CoV,
182 SARS-CoV, and SARS-CoV-2, contain highly stable, structured RNA regions throughout their
183 genomes. SARS-like coronavirus genomes were more highly structured than the MERS-CoV
184 genome, suggesting that even within the betacoronavirus family, RNA structuredness may be
185 unique to viral species. Importantly, SHAPE-MaP analysis recapitulated previously described
186 RNA structures⁵, providing confidence that SHAPE-MaP identifies bona fide RNA secondary
187 structures. Outside of structurally conserved noncoding regions of the genome, only a single
188 RNA structure was conserved across all three viruses. However, 65 conserved highly stable
189 structured regions were found that contained similar RNA structures when comparing SARS-
190 CoV and SARS-CoV-2 (**Supplementary Fig 3**). While some structures were conserved based
191 on sequence homology alone, the conservation in nearly a third of these structures appears to
192 be driven by structural conservation. Alignment and covariance analysis of >1000 SARS-CoV
193 and SARS-CoV-2 strains revealed greater levels of sequence conservation in SARS-like CoV
194 structured RNA regions, and maintenance of RNA secondary structures in highly stable
195 structures. This suggests these regions are under greater selective pressure than their non-
196 structured counterparts, and their likely importance in SARS-like coronavirus replication.

197 In contrast, we found distinct structural differences between MERS-CoV and the SARS-
198 like CoV, even within the known functional RNA structures (e.g. 5' and 3'UTR, ribosomal
199 frameshift element; **Fig 2A, 2C**). Such subtle, but distinct, changes in RNA structure could drive
200 phenotypic differences in replication of distinct virus species, even when those structures are
201 within conserved regions of RNA structure.

202 We also found significant conservation of both structuredness and RNA secondary
203 structures within the SARS-like CoV (**Fig 3A,B**). While much of this conservation was due to
204 sequence homology between the two viruses, we found that almost a third of conserved
205 structures show lower than average sequence homology as compared to the rest of the
206 genome, suggesting a functional role for RNA secondary structure (**Fig 3C**). Further, in

207 structures that did show high sequence homology, we found evidence of covariance
208 conservation of RNA structures, suggesting sequence variation constraints within the context of
209 an RNA structure. In conjunction with the fact that structured regions in SARS-CoV showed
210 lower sequence variance than non-structured regions, we hypothesize that RNA structuredness
211 and specific RNA secondary structures exert a selective pressure on sequence diversity. This
212 would suggest that these structures play important roles in SARS-like CoV replication, and
213 possibly pathogenesis. This suggests that disrupting these such conserved structures could be
214 a promising strategy for the development of live-attenuated vaccines. Understanding the
215 mechanism by which these novel RNA structures regulate SARS-CoV-2 replication could lead
216 to new antiviral therapeutic targets and inform rational vaccine design.

217

218 **References**

- 219 1. Salata C, Calistri A, Parolin C, et al. Coronaviruses: a paradigm of new emerging
220 zoonotic diseases. *Pathog Dis* 2019; 77 2020/02/18. DOI: 10.1093/femsdp/ftaa006.
- 221 2. Hui DSC and Zumla A. Severe Acute Respiratory Syndrome: Historical, Epidemiologic,
222 and Clinical Features. *Infect Dis Clin North Am* 2019; 33: 869-889. 2019/11/02. DOI:
223 10.1016/j.idc.2019.07.001.
- 224 3. Azhar EI, Hui DSC, Memish ZA, et al. The Middle East Respiratory Syndrome (MERS).
225 *Infect Dis Clin North Am* 2019; 33: 891-905. 2019/11/02. DOI: 10.1016/j.idc.2019.08.001.
- 226 4. Tse LV, Meganck RM, Graham RL, et al. The Current and Future State of Vaccines,
227 Antivirals and Gene Therapies Against Emerging Coronaviruses. *Front Microbiol* 2020; 11: 658.
228 2020/05/12. DOI: 10.3389/fmicb.2020.00658.
- 229 5. Yang D and Leibowitz JL. The structure and functions of coronavirus genomic 3' and 5'
230 ends. *Virus Res* 2015; 206: 120-133. 2015/03/05. DOI: 10.1016/j.virusres.2015.02.025.

231 6. Sheahan TP, Sims AC, Zhou S, et al. An orally bioavailable broad-spectrum antiviral
232 inhibits SARS-CoV-2 in human airway epithelial cell cultures and multiple coronaviruses in mice.
233 *Sci Transl Med* 2020; 12 2020/04/08. DOI: 10.1126/scitranslmed.abb5883.

234 7. de Wit E, Feldmann F, Cronin J, et al. Prophylactic and therapeutic remdesivir (GS-
235 5734) treatment in the rhesus macaque model of MERS-CoV infection. *Proc Natl Acad Sci U S*
236 *A* 2020; 117: 6771-6776. 2020/02/15. DOI: 10.1073/pnas.1922083117.

237 8. Gobalenya AE, Enjuanes L, Ziebuhr J, et al. Nidovirales: evolving the largest RNA virus
238 genome. *Virus Res* 2006; 117: 17-37. 2006/03/01. DOI: 10.1016/j.virusres.2006.01.017.

239 9. Ganser LR, Kelly ML, Herschlag D, et al. The roles of structural dynamics in the cellular
240 functions of RNAs. *Nat Rev Mol Cell Biol* 2019; 20: 474-489. 2019/06/12. DOI: 10.1038/s41580-
241 019-0136-0.

242 10. Madhugiri R, Fricke M, Marz M, et al. Coronavirus cis-Acting RNA Elements. *Adv Virus*
243 *Res* 2016; 96: 127-163. 2016/10/08. DOI: 10.1016/bs.aivir.2016.08.007.

244 11. Goebel SJ, Hsue B, Dombrowski TF, et al. Characterization of the RNA components of a
245 putative molecular switch in the 3' untranslated region of the murine coronavirus genome. *J*
246 *Virol* 2004; 78: 669-682. 2003/12/25. DOI: 10.1128/jvi.78.2.669-682.2004.

247 12. Plant EP and Dinman JD. The role of programmed-1 ribosomal frameshifting in
248 coronavirus propagation. *Front Biosci* 2008; 13: 4873-4881. 2008/05/30. DOI: 10.2741/3046.

249 13. Plant EP, Sims AC, Baric RS, et al. Altering SARS coronavirus frameshift efficiency
250 affects genomic and subgenomic RNA production. *Viruses* 2013; 5: 279-294. 2013/01/22. DOI:
251 10.3390/v5010279.

252 14. Cantara WA, Olson ED and Forsyth KM. Progress and outlook in structural biology of
253 large viral RNAs. *Virus Res* 2014; 193: 24-38. 2014/06/24. DOI: 10.1016/j.virusres.2014.06.007.

254 15. Siegfried NA, Busan S, Rice GM, et al. RNA motif discovery by SHAPE and mutational
255 profiling (SHAPE-MaP). *Nat Methods* 2014; 11: 959-965. 2014/07/17. DOI:
256 10.1038/nmeth.3029.

257 16. Smola MJ, Rice GM, Busan S, et al. Selective 2'-hydroxyl acylation analyzed by primer
258 extension and mutational profiling (SHAPE-MaP) for direct, versatile and accurate RNA
259 structure analysis. *Nat Protoc* 2015; 10: 1643-1669. 2015/10/02. DOI: 10.1038/nprot.2015.103.

260 17. Yang D, Liu P, Wudeck EV, et al. SHAPE analysis of the RNA secondary structure of the
261 Mouse Hepatitis Virus 5' untranslated region and N-terminal nsp1 coding sequences. *Virology*
262 2015; 475: 15-27. 2014/12/03. DOI: 10.1016/j.virol.2014.11.001.

263 18. Chen SC and Olsthoorn RC. Group-specific structural features of the 5'-proximal
264 sequences of coronavirus genomic RNAs. *Virology* 2010; 401: 29-41. 2010/03/06. DOI:
265 10.1016/j.virol.2010.02.007.

266 19. Di H, McIntyre AA and Brinton MA. New insights about the regulation of Nidovirus
267 subgenomic mRNA synthesis. *Virology* 2018; 517: 38-43. 2018/02/25. DOI:
268 10.1016/j.virol.2018.01.026.

269 20. Sola I, Moreno JL, Zuniga S, et al. Role of nucleotides immediately flanking the
270 transcription-regulating sequence core in coronavirus subgenomic mRNA synthesis. *J Virol*
271 2005; 79: 2506-2516. 2005/02/01. DOI: 10.1128/JVI.79.4.2506-2516.2005.

272

273

274

275

276

277

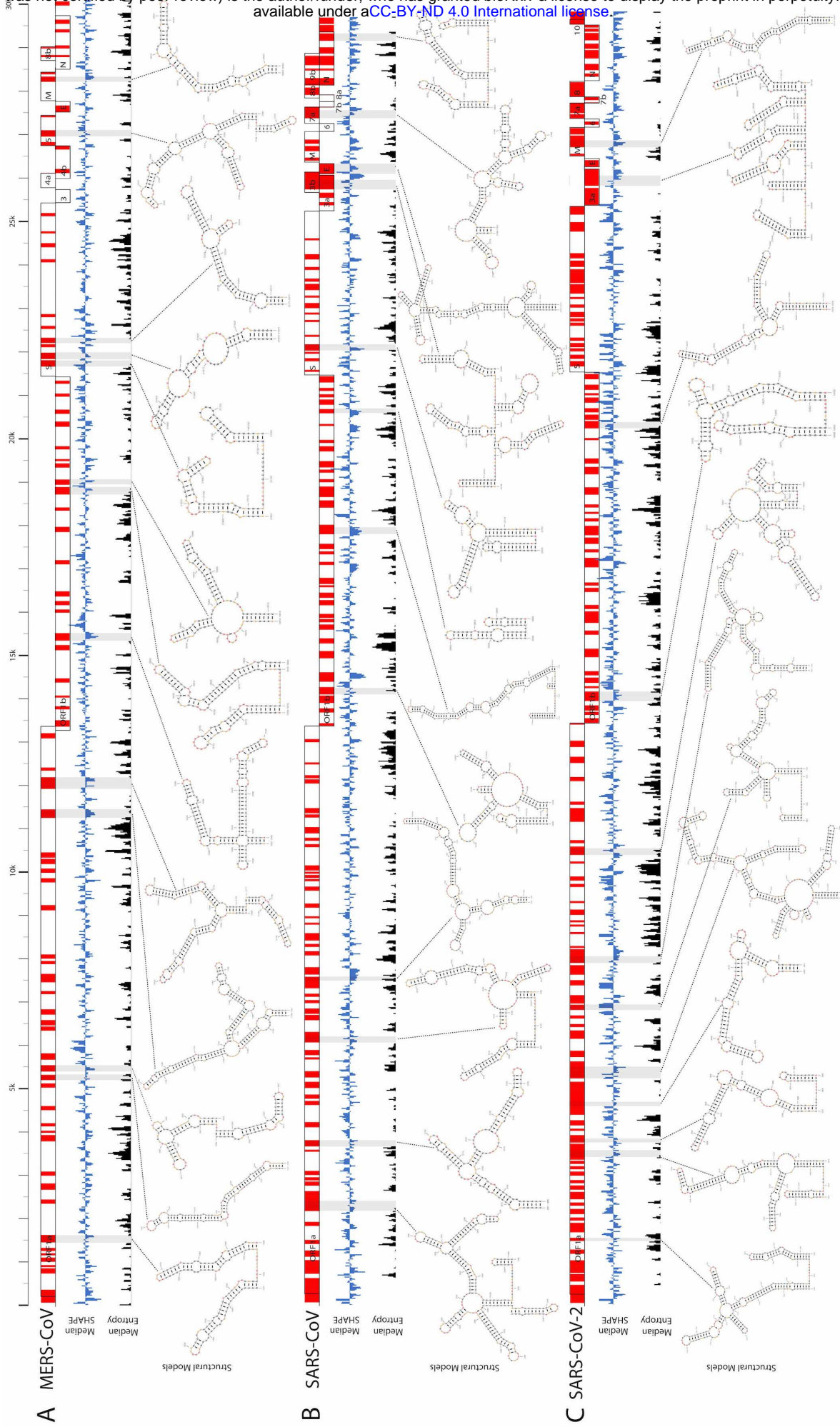
278

279

280

281

282 **Figures and Figure Legends**



284 **Figure 1. RNA secondary structure is pervasive throughout coronavirus genomes.**

285 Schematic of genome architecture for MERS-CoV (**A**), SARS-CoV (**B**), and SARS-CoV-2 (**C**).

286 Local median SHAPE reactivity (55-nt window) compared to the global median reactivity is

287 shown in blue. Median Shannon entropy (55-nt window) compared to the global entropy is

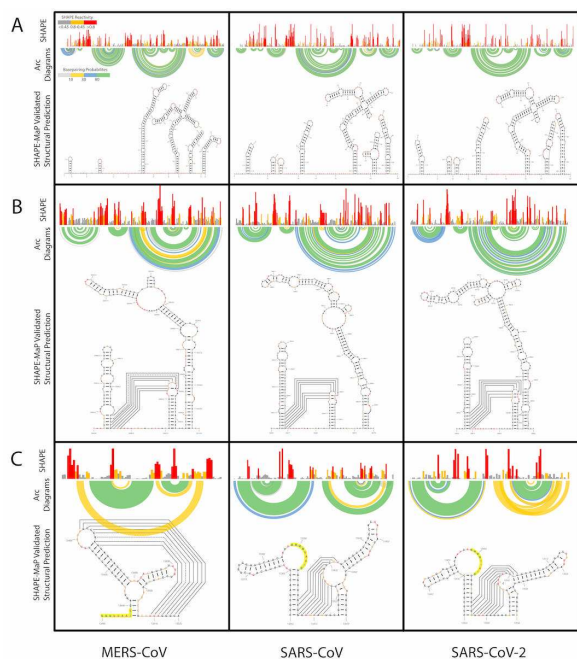
288 represented in black. Areas of significantly high RNA secondary structuredness (merged

289 SHAPE reactivity and Shannon entropy data, see Methods) are highlighted in red for each

290 genome. Examples of highly stable, RNA secondary structures are shown for each virus. Grey

291 bars below the genome schematics denote these structures are located.

292



293

294

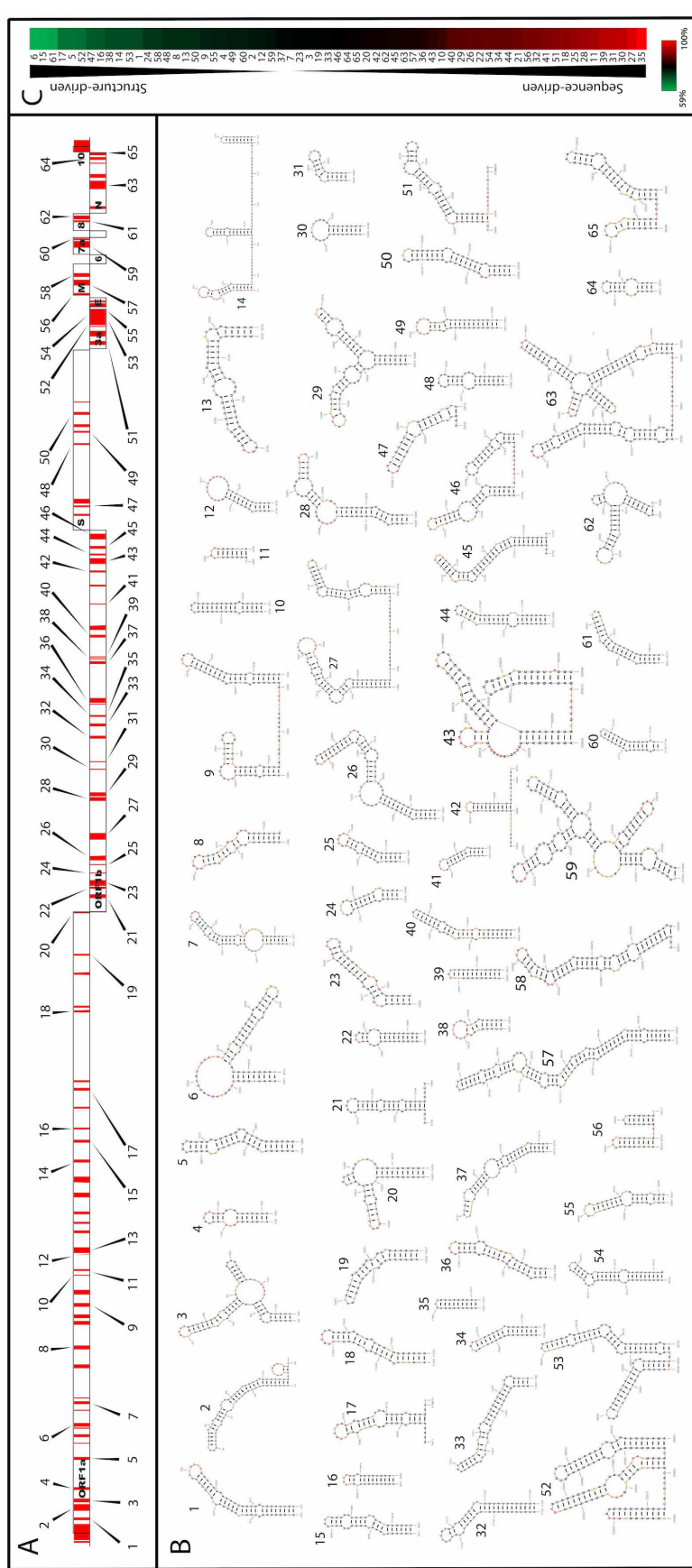
295 **Figure 2. Coronaviruses exhibit conserved secondary structure in functional RNA**

296 **elements.** SHAPE reactivity (top panel), base pair probability arc diagrams (middle panel), and
297 predicted RNA secondary structure models for the 5' UTR (**A**), 3' UTR (**B**), and structures
298 surrounding the programmed -1 ribosomal frameshift site (**C**) for MERS-CoV, SARS-CoV, and
299 SARS-CoV-2 are shown. Black connected lines represent previously described pseudoknot
300 tertiary interactions. The 'slippery sequence' that promotes ribosomal pausing is highlighted in
301 yellow.

302

303

304



305 **Figure 3. SARS-like CoV contain highly conserved regions of RNA structuredness. (A)**
306 SARS-CoV-2 genomic architecture schematic. Conserved regions of RNA structuredness
307 between SARS-CoV-2 and SARS-CoV are highlighted in red. Conserved highly stable RNA
308 secondary structures are denoted with arrows. (B) Representative structural models conserved,
309 highly stable RNA structures from (A) are shown. (C) The percent nucleotide conservation
310 between SARS-CoV and SARS-CoV-2 for each highly stable conserved RNA structure is shown
311 in a heat map. The highest conservation (100%) is shown in red, average nucleotide
312 conservation (79%) is represented in black, and the lowest conservation (59%) is shown in
313 green.

314

315 **Supplemental Files and Figures**

316 Supplemental Figure S1-S5

317 Supplemental Tables T1-T7

318

319 **Methods**

320 **Virus growth and purification.** MERS-CoV Jordan-N3/2012 isolate MG167 (accession
321 #KJ614529), was gown in Vero-81 cells. Vero-81 cells were cultured to ~80% confluence in
322 T175 flasks. Immediately prior to infection, the culture medium was aspirated and replaced with
323 Opti-MEM with 4% Hyclone FetalClone II (Cytiva). Cells were infected at a multiplicity of
324 infection (MOI) of 5 with MERS-CoV and were incubated at 37°C for 1 h. After 1 hour, cells were
325 aspirated, washed 1X with phosphate-buffered saline (PBS), and supplemented with fresh, pre-
326 warmed Opti-MEM with 4% FetalClone II. Cells were then incubated at 37°C for an additional 19
327 hours.

328 SARS-CoV Urbani isolate (accession #MK062179) and SARS-CoV-2 USA-W1/2020
329 isolate (accession #MN985325) were gown in Vero E6 cells. Vero E6 cells were culture to ~90%

330 confluence in T175 flasks. Immediately prior to infection the culture medium was aspirated and
331 cells were washed with PBS. Flasks were infected at an MOI of 5 with SARS-CoV and MOI of 3
332 for SARS-CoV-2 at 37°C for 1 hour. After 1 hour cells were supplemented with pre-warmed
333 DMEM with 5% FetalClone II. Cells were then incubated for an additional 24 hours at 37°C.
334 To isolate virion RNA, cell supernatant was aspirated and concentrated using Amicon Ultra
335 Centrifugal Filters (Millipore Sigma) to approximately 4 mL total volume. The supernatant was
336 then lysed in TRIzol LS (Invitrogen), and viral RNA pellets were harvested according to the
337 manufacturer's suggested protocol. RNA was extracted from the TRIzol using chloroform
338 followed by overnight precipitation at -20°C.

339

340 **SHAPE modification and library generation.** Modified RNA was folded at 37°C in the
341 presence of 10 mM MgCl₂ and 111 mM KCl for 15 minutes, flowed by a 5-minute treatment of
342 100 nM 1-methyl-7-nitroisatoic anhydride (1M7) also at 37°C. Unmodified RNA was folded under
343 the same conditions as the modified RNA and treated with DMSO for 5 minutes at 37°C. The
344 denatured control RNA was incubated at 90°C for 2 minutes followed by a 2-minute treatment of
345 100 nM 1M7 at 95°C. Following all treatments, RNAs were purified using the RNA Clean &
346 Concentrator -5 Kit (Zymo Research). Purified RNAs were random primed using Random
347 Primer 9 (NEB) by incubation at 65°C for 5 minutes followed by rapid cooling on ice. They were
348 then mixed with a master mix that consisted of 10 mM dNTPs, 0.1 M DTT, 500 mM Tris pH 8.0,
349 750 mM KCl, 500 mM MnCl₂, and SuperScript II Reverse Transcriptase (Thermo Fisher
350 Scientific). They were incubated at 25°C for 15 minutes, 42°C for 180 minutes, followed by a
351 heat inactivation at 70°C for 15 minutes. After reverse transcription they were then cleaned
352 using Illustra MicroSpin G-50 columns (GE Healthcare), double stranded DNA (dsDNA) was
353 generated by use of NEBNext Ultra II Non-Directional RNA Second Strand Synthesis Module

354 (NEB), purified using PureLink PCR Micro Kit (Thermo Fisher Scientific), and dsDNA was
355 quantified using Qubit dsDNA HS Assay Kit (Thermo Fisher Scientific).

356 Libraries were prepared using Nextera XT DNA Library Preparation Kit (Illumina),
357 cleaned using a 1:0.6 ratio of Agencourt AMPure XP (Beckman Coulter), and quantified again
358 using Qubit dsDNA HS Assay Kit following manufacturer's recommended protocol in each case.
359 Libraries were sequenced on a MiSeq Desktop Sequencer (Illumina) using a MiSeq Reagent Kit
360 v3 (600-cycle) (Illumina)^{1,2}.

361

362 **Structural prediction.** Sequenced reads from the unmodified RNAs were aligned to the
363 reference sequences downloaded from NCBI to correct viral sequences for potential mutations.
364 SHAPE reactivities were derived using the ShapeMapper Pipeline v1.2. Structural predictions
365 and Shannon entropy were obtained using Superfold v1.0 with a maximum pairing distance of
366 500 base pairs to calculate minimum free-energy models using SHAPE reactivities as folding
367 constraints. Highly stable structured regions were predicted based on 55 base pair rolling
368 averages of SHAPE reactivity (<0.3) and Shannon entropy (<0.04). Highly stable structured
369 regions were expanded to encompass full base pairing regions as needed³. Specific structure's
370 minimum free energy models were generated using RNAstructure's Fold v6.0.1 using standard
371 settings and incorporating SHAPE reactivities as folding constraints⁴.

372

373 **Covariation and alignments.** Homologous structures were found and base pairs with
374 significant covariation were identified as in *Kutchko et al*¹. Briefly, homologous structures were
375 identified using the Infernal software suite v1.1.2⁵. A model was built for each structure using
376 cmbuild and cmcalibrate. All available MERS-CoV (350 genomes), SARS-CoV (140 genomes),
377 and SARS-CoV-2 (1,524 genomes) sequences available on ViPR on 5-12-2020 were searched
378 for similar structures using cmsearch with -A option to automatically generate an alignment.
379 Base pairs with significant covariance were identified using R-scape program v1.2.3⁶.

380 MUSCLE alignments were performed on the CLC Genomics Workbench v12.0.3
381 (Qiagen) module Additional Alignments v1.9 for mutational frequency identification using the
382 above mentioned ViPR sequences. Genomes containing gaps (>5 nucleotides) or multiple
383 unidentified nucleotides were excluded from alignments. ClustalOmega alignments were
384 performed using EMBL-EBI for individual viral genome comparisons⁷.

385
386 **Sequence conservation and structuredness.** A sequence conservation score, ranging from 0
387 to 1, was calculated at each aligned genomic position after insertions and deletions were
388 removed from the alignment. Whole genome conservation was calculated based on an average
389 of each position's conservation score across the entire genome and also the average of 67 base
390 pair rolling windows across the entire genome. Structuredness was calculated at each
391 nucleotide position by adding the SHAPE reactivity value to Shannon entropy value, both
392 normalized to their mean value over the entire genome. This was used to create a ranking of
393 each highly stable structured regions. Statistical analysis was performed using ANOVA: Single
394 factor.

395

396 **Methods References**

397

398 1. Kutchko KM, Madden EA, Morrison C, et al. Structural divergence creates new
399 functional features in alphavirus genomes. *Nucleic Acids Res* 2018; 46: 3657-3670. 2018/01/24.
400 DOI: 10.1093/nar/gky012.

401 2. Smola MJ, Rice GM, Busan S, et al. Selective 2'-hydroxyl acylation analyzed by primer
402 extension and mutational profiling (SHAPE-MaP) for direct, versatile and accurate RNA
403 structure analysis. *Nat Protoc* 2015; 10: 1643-1669. 2015/10/02. DOI: 10.1038/nprot.2015.103.

404 3. Siegfried NA, Busan S, Rice GM, et al. RNA motif discovery by SHAPE and mutational
405 profiling (SHAPE-MaP). *Nat Methods* 2014; 11: 959-965. 2014/07/17. DOI:
406 10.1038/nmeth.3029.

407 4. Reuter JS and Mathews DH. RNAstructure: software for RNA secondary structure
408 prediction and analysis. *BMC Bioinformatics* 2010; 11: 129. 2010/03/17. DOI: 10.1186/1471-
409 2105-11-129.

410 5. Nawrocki EP and Eddy SR. Infernal 1.1: 100-fold faster RNA homology searches.
411 *Bioinformatics* 2013; 29: 2933-2935. 2013/09/07. DOI: 10.1093/bioinformatics/btt509.

412 6. Rivas E, Clements J and Eddy SR. A statistical test for conserved RNA structure shows
413 lack of evidence for structure in lncRNAs. *Nat Methods* 2017; 14: 45-48. 2016/11/08. DOI:
414 10.1038/nmeth.4066.

415 7. Madeira F, Park YM, Lee J, et al. The EMBL-EBI search and sequence analysis tools
416 APIs in 2019. *Nucleic Acids Res* 2019; 47: W636-W641. 2019/04/13. DOI: 10.1093/nar/gkz268.

417

418 **Acknowledgements**

419 We would like to thank the Moorman, Baric, and Heise labs for helpful conversations. This work
420 was supported by the following grants from the National Institute of Allergy and Infectious
421 Disease: AI137887 and AI138056 to N.J.M. and M.T.H., AI108197 to R.S.B., and support from
422 T32 AI007419 to E.A.M. and E.J.F.

423

424

425

426 **Author Contributions**

427 W.S., M.T.H., R.S.B., and N.J.M. conceptualized the work; W.S., E.J.F., and R.L.G. acquired
428 data. W.S., E.A.M., and N.J.M. analyzed data; W.S., H.A.V., and N.J.M. drafted and revised the
429 manuscript.

430

431 **Competing Interest Declaration**

432 The authors declare they have no competing interests.

433

434 **Additional Information**

435 Supplementary Information is available for this paper.

436 Correspondence and requests for materials should be addressed to Nathaniel J. Moorman.